Towards Modeling Phase Center Variations for Multi-Frequency and Multi-GNSS

Tobias Kersten*, Steffen Schön

Abstract
With the Hannover concept of absolute field calibration of GNSS antennae the determination of receiver antenna Phase Center Variations (PCV) can be done routinely for the GPS and GLONASS L1 and L2 frequencies, respectively. The need of multi-GNSS and multi-frequency applications - demanded by a broader navigation community - tends to a combined estimation of receiver antenna depending properties for various frequencies and systems. This approach is only advantageous if inter-frequency and inter-system biases are known and continuously considered.
In this contribution we investigate steps towards a concept for multi-system-calibration. After a short introduction to the absolute field calibration procedure, the mathematical model as well as adjustment concept will be presented. We show that test results suggest that the receiver demodulation may have an impact on the estimated PCV.
The correlation analysis of the multi-frequency multi-GNSS approach underlines that (1) the correct consideration of the mathematical correlations between the parameters to up to 25%, (2) The receiver clock links the results from different frequencies and (3) PCV for different GNSS systems can be computed in a common adjustment since the inter-system correlations are below 1-2%.

Keywords
antenna calibration — GNSS — phase centre variation (PCV)

Institut für Erdmessung, Leibniz University Hannover, Lower Saxony, Germany
***Corresponding author**: kersten@ife.uni-hannover.de

Contents

Introduction 1
1 Receiver dependent Aspects 2
1.1 Experimental Set-up 2
1.2 Processing Strategy 3
1.3 Results of the Calibration Experiments 3
2 Modelling and Estimation of PCV Parameters 4
2.1 Observation Model 4
2.2 Mathematical Formulation 5
2.3 Correlation Analysis 5
2.4 Impact of Covariance Information 6
Acknowledgements 8
References 8

Introduction

In many applications precise positioning is required with an accuracy level that demands to consider systematic errors of the receiver antenna itself. These effects are caused by inhomogeneities of the electrical phase center of the receiver antennae. They are parameterized by:

1. the vector between the physically well defined antenna reference point (ARP) and the mean phase center, i.e. the phase center offset (PCO),
2. an azimuth α and elevation $e = \pi/2 - z$ depending phase correction $\Delta\phi(\alpha, z)$, where z denotes the zenith angle.

Then the phase center variations (PCV) are described in an antenna system $[\vec{e}_i]_{ant}$ with its origin at the ARP. The base vector $[\vec{e}_1]_{ant}$ points to the antenna north marker, $[\vec{e}_2]_{ant}$ to the east, and $[\vec{e}_3]_{ant}$ completes $[\vec{e}_1]_{ant}$ and $[\vec{e}_2]_{ant}$ to a left-hand coordinate system. Assuming a well levelled and orientated antenna, the antenna's coordinate system coincides with the local topocentric system. Then the antenna frequency depending PCV pattern is the variation between an ideal spherical and a real measurable phase front, parameterized in terms of the azimuth α and zenith angle z of the line-of-sight $[\vec{e}]^j$ for a satellite j, cf. Figure 1.

$$PCV(\alpha, z) = [\vec{e}_i]^j \cdot PCO + \Delta\phi(\alpha, z) \tag{1}$$

Each antenna has its individual features. Consequently the variations are individual and should be tested for every antenna model and frequency, respectively.

PCVs were determined successfully and routinely since 2000 by the Hannover concept of absolute field calibration

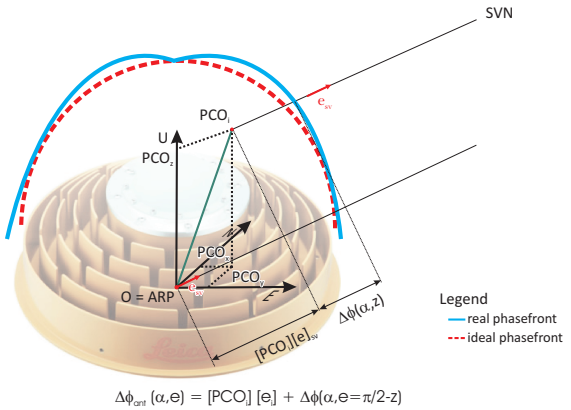

Figure 1. Geometric relations of PCV.

as described in detail in [1]. This approach uses the actually available, modulated GNSS signals in the field while calibration in anechoic chambers rely on synthetic signals, cf. [2] and [3].

Fundamental discussions by [4] and [5] as well as [6] and [7], to note only few, contributed to the international acceptance of absolute PCVs. Since 2005 they are an an international standard not only for the International GNSS Service (IGS), but also for global and regional geodetic network applications, like e.g., the EPN (EUREF Permanent GNSS Network), [8] or SAPOS (Satellite Positioning Service of the Federal Republic of Germany).

Individual, absolute phase center variations are up to now determined irrespectively of the receiver in use. However it can be expected that receiver depending properties have a, perhaps significant, impact on the estimated PCVs.

This situation will further accentuate in multi-GNSS and multi-frequency receivers.

On the one hand it is well known that already for GPS L2, individual internal tracking algorithms, depending on the manufacturer are applied for signal acquisition and tracking.

For Galileo variations and different observations are provided to the user of high end equipment depending on the manufacture's tracking strategy. For example the *Javad Delta TRE-G3T* receiver, used as standard equipment in our applications, tracks all public GPS/GLONASS signals as well as Galileo. The signals E1 and E5a are tracked by a combined tracking loop. Otherwise the E1 CBOC signal from GIOVE A/B is tracked by a combined tracking loop for BOC(1,1) and BOC(6,1) with a proprietary correlator technique. However for instance the used LEICA receiver GRX1200+GNSS provides the tracking of GPS, GLONASS and SBAS as well as GIOVE A and B. The GRX receiver supports the codes on L1 C/A and L2C as well as carrier phases L1 P, L2 P(Y) and L5. In addition GIOVE signals E1-B&C and E5a-I&Q as well as E5b-I&Q and E5ab AltBOC can be tracked with a prototype of the firmware. This situation of multi-frequency receiver will further accentuate with new upcoming signals, where each receiver uses specific and proprietary demodulation schemes.

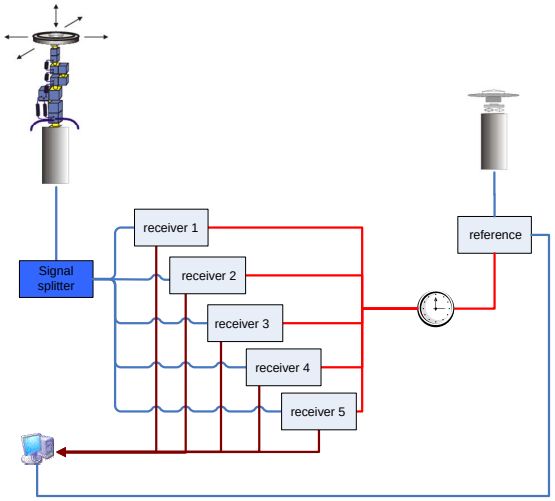

Figure 2. Common clock experiments to analyse the impact of different receiver equipment on the estimated Phase Center Variations.

On the other hand GLONASS does not permits the access to the precise P code on both frequencies since this code with a length of more than 33 Mio. chips was decrypted in 1989 by some scientists [9]. Based on the fact that GLONASS uses Frequency Division Multiple Access (FDMA) to identify the corresponding satellite, the frequencies are defined as follows,

$$\begin{aligned} L_1 &: f_1 = 1602 + k \cdot 9/16\,\text{MHz},\ \lambda = 19\,\text{cm}, \\ L_2 &: f_2 = 1246 + k \cdot 7/16\,\text{MHz},\ \lambda = 24\,\text{cm}, \end{aligned} \tag{2}$$

with k being the frequency channel number with a range of $k = (-7,\ldots,+6)$. The difference of mean GLONASS and GPS carrier phase frequency is ≈ 22MHz for the actual GLONASS constellation. Therefore GLONASS PCV were long times replaced by GPS PCV. Now GLONASS PCV are considered for a mean frequency.

In this contribution we focus on the functional modeling of receiver antenna PCV. In a first part we analyse the impact of different receiver on the calibration results of high end GNSS antennae. To this end calibration experiments were carried out using the Hannover concept of absolute field calibration. We used several reference station receivers in combination with different reference station antennae which show high repeatability of individual PCV determination although geometric properties differ. In a second part we review the mathematical model of PCV estimation in order to extend it properly for a multi-frequency and multi-GNSS approach.

1. Receiver dependent Aspects

1.1 Experimental Set-up

For our tests, the set of widely used reference station equipment is shown in table 1. All receivers support the tracking of actual GPS as well as GLONASS L1 and L2 frequencies. To reduce the impact of the individual receiver clock error, an

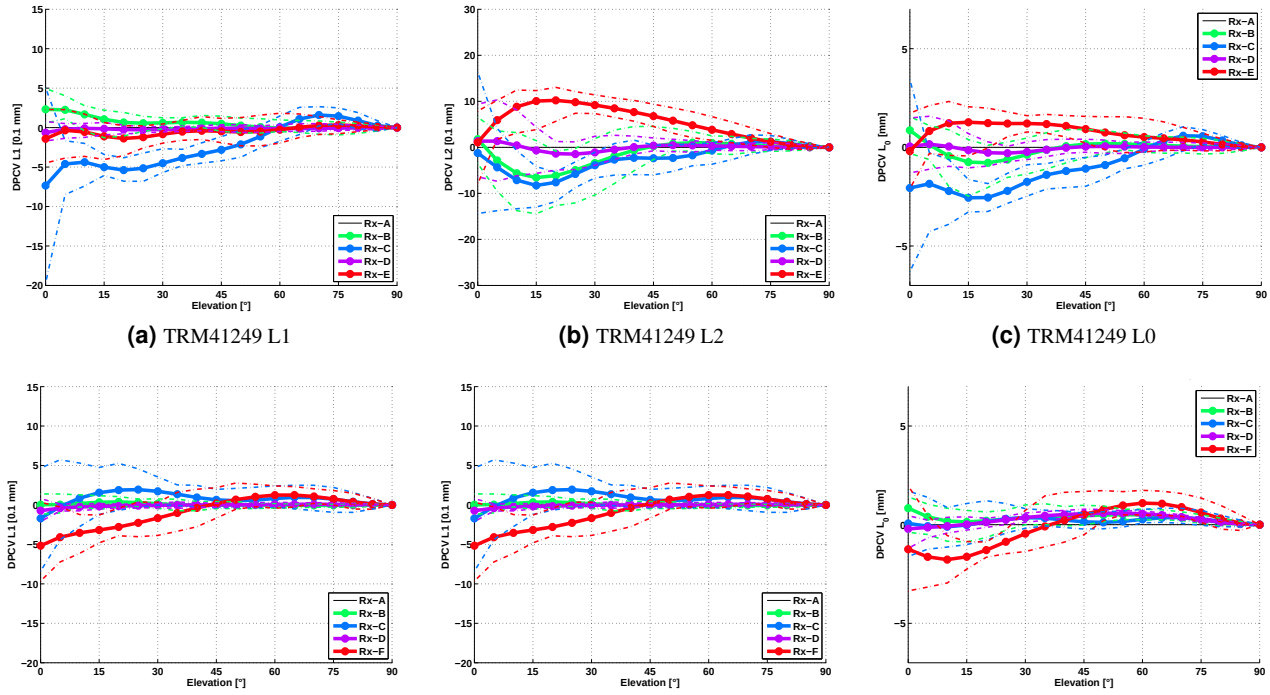

(a) TRM41249 L1 **(b)** TRM41249 L2 **(c)** TRM41249 L0

(d) LEICA AR25 R2 L1 **(e)** LEICA AR25 R2 L2 **(f)** LEICA AR25 R2 L0

Figure 3. Impact of several reference station equipment on GPS PCV estimation. The dotted lines show the minimum and maximum variations in azimuth respectively.

Table 1. GNSS reference station Equipment used during the analysis.

antenna		frequency
Trimble Zephyr Geodetic I	GPS	L1 L2
	GLO	L1 L2
Leica AR25 R2 LEIT	GPS	L1 L2 L5
	GLO	L1 L2 L3
	GAL	E2-L1-E1 E5a,b E6 AltBOC
Leica AR25 R3 LEIT	GPS	L1 L2 L5
	GLO	L1 L2 L3
	GAL	E2-L1-E1 E5a,b E6 AltBOC
Topcon CRG3 SCIS	GPS	L1 L2 L5
	GLO	L1 L2

receiver	frequency
Javad DELTA TRE-G3T	GPS L1/L2/L5, GLO L1/L2, GAL E1/E5
JPS LEGACY	GPS L1/L2, GLO L1/L2
LEICA GRX1200+GNSS	GPS L1/L2/L5, GLO L1/L2 GAL E1/E5ab
Septentrio AsteRx2DR	GPS L1/L2, GLO L1/L2
Topcon NET G3A	GPS L1/L2/L5, GLO L1/L2
Trimble NETR8	GPS L1/L2, GLO L1/L2

external rubidium frequency standard was used as a common clock. The set up is depicted in Figure 2.

All receiver were connected to one antenna in a sense of a zero baseline and calibration values were calculated simultaneously for every unit. The processing and control is performed by an external PC.

For a meaningful determination of PCV parameters the precise robot was calibrated. Calibrations were done with a LEICA laser tracker LTD 640 at the Geodetic Institute, Leibniz University Hannover (GIH) using an economic distribution of significant robot positions. Parameters like arm length or angle offsets were determined and applied to the robot. Therefore the robot can reach an accuracy of approximate 0.25 mm for every position.

To reach the right signal strength at the Trimble *Zephyr Geodetic I* antenna, a special power supply was used to feed the antenna with 125 mA whereby the *Javad Delta TRE-G3T* receiver only supports 100 mA.

1.2 Processing Strategy

A standard PCV determination with the Hannover concept of absolute field calibration is used. Within this process GNSS measurements were carried out with an antenna mounted on a precise robot. The antenna is rotated and tilted underneath the current GNSS constellation. Measurements of up to 6000-8000 epochs in 6-8 hours were done whereby the antenna is rotated and tilted around one virtual point, the a priori mean PCO. To perform a homogeneous distribution of measurements over the antenna's hemisphere, the orientation of the antenna changes on subsequently epochs.

In standard analysis the PCVs obtained from each receiver were described by spherical harmonics with an expansion of degree $n = 8$ and order $m = 5$ to determine elevation as well as azimuth depending variations.

Please note that the description of PCV according to Fi-

gure 1 has several degrees of freedom. Without loss of generality and for a consistent comparison of different PCVs, the values have to be transformed to one common PCO and were then re-centered at zenith to zero. Therefore the PCO obtained from the calibration with *Javad Delta TRE-G3T* serves as reference. Finally the ΔPCV were calculated with respect to the PCV obtained from *Javad Delta TRE-G3T*, used as reference.

1.3 Results of the Calibration Experiments

Some results of the experiments for two antennae are shown in Figure 3 for GPS and in Figure 4 for GLONASS, respectively. Equipment depending variations appear although equal settings (tracking loops, etc.) and a common clock were applied.

For GPS L1 the variations are in a range of up to $0.5-0.8$ mm and therefore hard below the significance level of 0.3 mm provided by the precise calibration unit itself.

As depicted in Figure 3b and 3e the variation on GPS L2 are obviously in a band of $1-1.2$ mm. The enhanced variations spectra on GPS L2 are explainable by the proprietary tracking algorithms for the P(Y) code. Although the elevation depending variations are in a range of 1 mm, the azimuth depended variations are smaller than 0.5 mm over the elevation range.

By forming the ionosphere free linear combination the characteristics are dominated by the L2 signal and are in a range of 2 mm.

For GLONASS, the variations on the frequency L1 are within a range of $0.5-0.8$ mm (cf. Figure 4a and 4d) and hereby in the same range as for GPS. Individual characteristics can be assigned to the individual antenna.

Based on the fact that both precision codes on the GLONASS frequencies are unencrypted, the variations are more homogeneous in combination with different receivers. The differences which are detectable at zero elevation (cf. Figure 4b and 4e) reflects to the different estimated PCO, which differ up to 1 mm. As it is noticeable from Figure 4 the variantions of the ΔPCV are more homogeneous than those determined for GPS (cf. Figure 3).

The ionosphere free linear combination for GLONASS shows a similar behaviour with maximal variations of up to 2 mm at elevations $\geq 30^\circ$ as shown in Figures 4c and 4f.

From these first investigations we can see that small but significant receiver depending variations exist. It can be expected that for the new and upcoming signals the differences will increase due to different demodulation schemes. To be prepared for multi-frequency, multi-GNSS applications the Hannover concept of the absolute and individual antenna calibration must be extended. In parallel we review the current methodology.

2. Modelling and Estimation of PCV Parameters

2.1 Observation Model

To get access to the observables we take a short look to the undifferenced phase observation $\Phi^j_{f_A}$ in meters for the frequency f from station A to satellite j.

$$\begin{aligned}\Phi^j_{f_A} = &\rho^j_A + c(\delta t_A - \delta t^j) + \lambda_f N_{f_{A,B}} \\ &+ (\delta\varphi_{f_A} - \delta\varphi^j_f) + T^j_{f_A} - I^j_{f_A} \\ &+ MP^j_{f_A} + PCV_{f_A} + \varepsilon^j_{f_A},\end{aligned} \tag{3}$$

with the geometric distance ρ^j_A, the speed of light c, the receiver and satellite clock error δt_A and δt^j resp., the tropospheric $T^j_{f_A}$ and ionospheric $I^j_{f_A}$ delay, the ambiguity term N_{f_A} the hardware delays in receiver ($\delta\varphi_{f_A}$) and satellite ($\delta\varphi^j_f$) the phase multipath term $MP^j_{f_A}$, the phase center variations PCV_{f_A} and additional measurement noise $\varepsilon^j_{f_A}$.

$$SD^j_{A,B}(t_\iota) = \Phi^j_{f_A} - \Phi^j_{f_B} \tag{4}$$

By forming single differences $SD^j_{A,B}(t_\iota)$ on a short baseline of approximate 8 m between stations A and B at every epoch t_ι effects introduced by the satellite and by distance depending factors are nearly eliminated. Applying time differences to the single differences from equation (4) like

$$\Delta SD^j_{f_{A,B}}(t_\iota) = SD^j_{f_{A,B}}(t_{\iota+1}) - SD^j_{f_{A,B}}(t_\iota) \tag{5}$$

we obtain access to the observation equation for each frequency

$$\begin{aligned}\Delta SD = &c\cdot\Delta\delta t_{A,B}(t_\iota,t_{\iota+1}) + \Delta PCV^j_A(t_\iota,t_{\iota+1}) \\ &+ \Delta MP^j_{A,B}(t_\iota,t_{\iota+1}) + \Delta d^j_{A,B}(t_\iota,t_{\iota+1}) \\ &+ \Delta T^j_{A,B}(t_\iota,t_{\iota+1}) - \Delta I^j_{AB}(t_\iota,t_{\iota+1}) \\ &+ \Delta\rho^j_{AB}(t_\iota,t_{\iota+1}) + PWU^j_A(t_\iota,t_{\iota+1})\end{aligned} \tag{6}$$

with the differential receiver clock error $c\cdot\Delta\delta t_{A,B}(t_i,t_{i+1})$, the topography of PCV pattern $\Delta PCV^j_A(t_\iota,t_{\iota+1})$ considered in the mathematical formulation (9) and the additional differential error terms. Due to the short time offset between consecutive epochs of maximal 5 sec and the short station seperation of approximate 8 m, the terms $\Delta T^j_{f_{A,B}}(t_\iota,t_{\iota+1})$ and $\Delta I^j_{f_{A,B}}(t_\iota,t_{\iota+1})$ vanish. In addition, the ambiguity term is eliminated as well as the PCV pattern on station B. The multipath term at station B is also eliminated and at the station A largely reduced .

The internal receiver depended hardware delay is up to now not modelled and assumed to be below the significance level of 0.25 mm.

It is obviously that PCV information for the antenna under test at station A on the robot can only be determined by changing the antenna orientation between subsequent epochs. The phase wind up correction $PWU^j_A(t_\iota,t_{\iota+1})$ according to [10] has to be considered as a result of the rotation of a tilted antenna, which is carried out with the precise robot. Station coordinates as well as satellite coordinates are held fixed.

The differential geometric range $\Delta\rho^j_{AB}(t_\iota,t_{\iota+1})$ is influenced by the robot model itself. The corrections were determined by a precise calibration of the robot with a LEICA laser

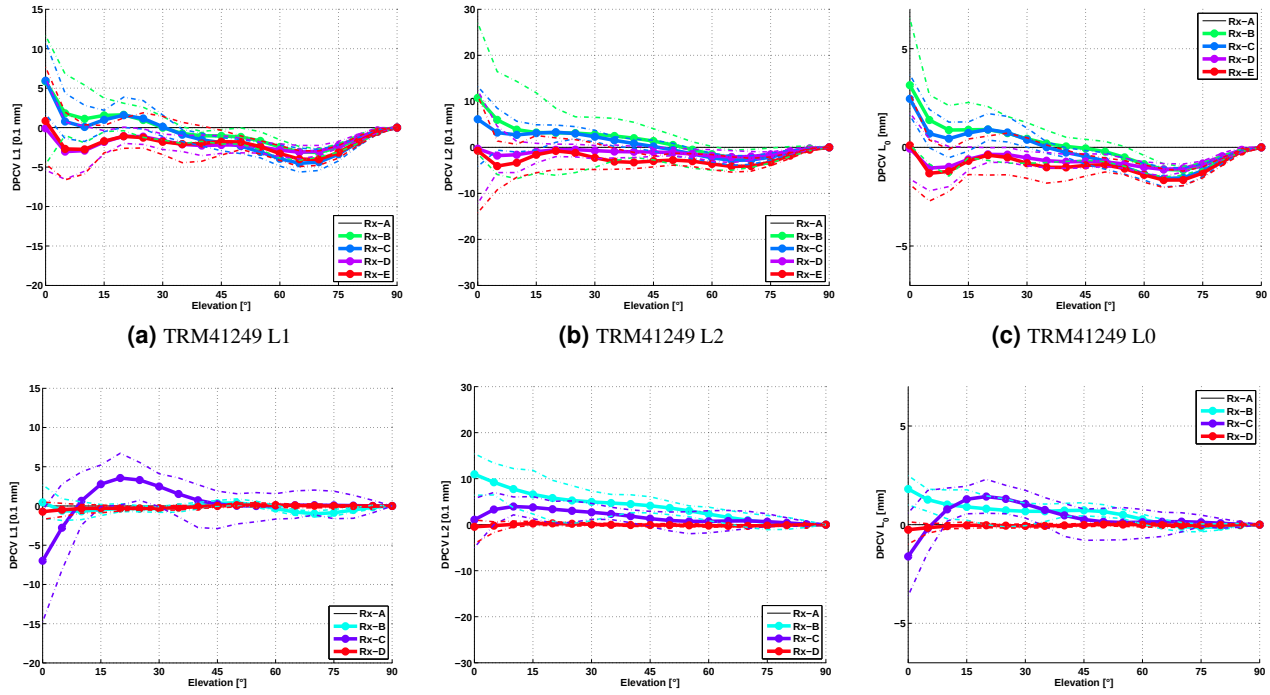

(a) TRM41249 L1 **(b)** TRM41249 L2 **(c)** TRM41249 L0

(d) LEICA AR25 R2 L1 **(e)** LEICA AR25 R2 L2 **(f)** LEICA AR25 R2 L0

Figure 4. Impact of several reference station equipment on GLONASS PCV estimation. The dotted lines showing the minimum and maximum variations in azimuth respectively.

tracker LTD 640 in a laboratory to the 0.25 mm level. The correction values for angle offsets, arm length of robot modules, weighting coefficients and module defined offsets were determined and directly applied to the robot control. For some constellation of modules the deviation from the nominal position can reach up to $10-13$ mm if the corrections were not applied. The accuracy to reach the same point under different module constellations is 0.25 mm.

2.2 Mathematical Formulation

Based on the physical characteristics of the receiver antenna as an omni-directional/spherical radiator it is obvious to describe variations from this ideal surface by an expansion over a sphere.

As already discussed at equation (6) the PCV pattern of the antenna under test can only be determined by changing the orientation in azimuth $\alpha_0+\Delta\alpha$ and zenith $z=z_0+\Delta z$ between subsequently epochs $t_\iota, t_{\iota+1}$.

$$f(\alpha,z)=PCV(\Delta\alpha,\Delta z,t_{\iota+1})-PCV(\alpha_0,z_0,t_\iota) \tag{7}$$

An arbitrary function $PCV(\alpha,z)$ can be expand into a series of fully normalized harmonics as described in the following. A very good introduction is given by [11].

$$\begin{aligned} PCV(\alpha,z) &= \sum_{n=0}^{n_{Max}}\sum_{m=0}^{m=n}\left\{\bar{A}_{nm}\bar{R}_{nm}(\alpha,z)+\bar{B}_{nm}\bar{S}_{nm}(\alpha,z)\right\} \\ \begin{Bmatrix}\bar{R}_{nm}(\alpha,z)\\ \bar{S}_{nm}(\alpha,z)\end{Bmatrix} &= \begin{Bmatrix}\cos(m\alpha)\\ \sin(m\alpha)\end{Bmatrix} N_{nm}P_{nm}(\cos(z)) \end{aligned} \tag{8}$$

with fully normalized spherical harmonic functions $\bar{R}_{nm}(\alpha,z)$ and $\bar{S}_{nm}(\alpha,z)$, the degree n and order m of expansion, the zenith angle z and azimuth α of a satellite in the topocentric system as defined in (1), the normalization factor N_{nm}, the associated Legendre functions $P_{nm}(\cos(z))$, and finally the unknown fully normalized spherical harmonic coefficients $\bar{A}_{nm}$ and $\bar{B}_{nm}$, [11].

This approach is physically meaningful since variations in elevation as well as in azimuth are considered. To prevent singularity of the normal equation system (NEQS) one has to keep in mind, that the absolute element $\bar{A}_{00}$ cannot be estimated since it is an unknown scale factor, the coefficients $\bar{B}_{n0}$ are equal zero since $\sin(0\cdot\alpha)=0$ and that the PCV are centered in the zenith to zero, $\mathrm{PCV}(\alpha,z=0):=0$.

The unknown parameter $\bar{A}_{nm}$ and $\bar{B}_{nm}$ are determined by a least squares adjustment

$$\mathbf{l_j}+\mathbf{v_j}=\mathbf{A_j}\mathbf{x}, \tag{9}$$

with the vector $\mathbf{l_j}$ of observations, the residual vector $\mathbf{v_j}$, the Jacobi matrix $\mathbf{A_j}$ and the unknown vector $\mathbf{x}$. The index j denote the aggregation of observations to satellite j over epochs t_ι. This common adjustment problem is solved by

$$\begin{aligned} \mathbf{x} &= \left(\sum_j\left\{\mathbf{A_j^T}\mathbf{P_j}\mathbf{A_j}\right\}\right)^{-1}\sum_j\left\{\mathbf{A_j^T}\mathbf{P_j}\mathbf{l_j}\right\} \\ &= \mathbf{N^{-1}}\mathbf{n}, \end{aligned} \tag{10}$$

with the weighting matrix of observables $\mathbf{P_j}$, the NEQS matrix

$\mathbf{N}$ and the absolute term $\mathbf{n}$. For a combination of different frequencies in one common adjustment (10) can be easily expand to block matrices.

In the following GPS L1 is parameterized in a matrix $\mathbf{A_1}$ and GPS L2 in a matrix $\mathbf{A_2}$, respectively. The NEQS is generated sequentially for every epoch and satellite with different antenna orientations as described by (10). This approach results into the following NEQS considering a differential receiver clock error for every epoch (matrix $\mathbf{B}$).

$$\mathbf{N} = \begin{bmatrix} \mathbf{A_1^T P_1 A_1} & \mathbf{0} & \mathbf{A_1^T P_1 B_1} \\ \mathbf{0} & \mathbf{A_2^T P_2 A_2} & \mathbf{A_2^T P_2 B_2} \\ \mathbf{B_1^T P_1 A_1} & \mathbf{B_2^T P_2 A_2} & \mathbf{B_1^T P_1 B_1 + B_2^T P_2 B_2} \end{bmatrix} \tag{11}$$

Depending on the receiver clock behaviour also different models could be possible, like e.g. polynomial clock models as well as frequency depending receiver clock modelling.

2.3 Correlation Analysis

To prevent an over-parametrization in a formulation for multi-GNSS multi-frequency a closer look to the impact of additional unknowns onto the estimation parameters is needed. The differential receiver clock errors can be eliminated from equation (11). For this we combine the NEQS in the following way,

$$\begin{bmatrix} \mathbf{N_{11}} & \mathbf{N_{12}} \\ \mathbf{N_{21}} & \mathbf{N_{22}} \end{bmatrix} \begin{bmatrix} \mathbf{x_1} \\ \mathbf{x_2} \end{bmatrix} = \begin{bmatrix} \mathbf{n_1} \\ \mathbf{n_2} \end{bmatrix}, \tag{12}$$

with $\mathbf{N_{11}}$ being the NEQS of the unknowns for one GNSS system and both frequencies, $\mathbf{N_{22}}$ including all differential clock parameters.

To eliminate unnecessary parameters from (12) we first build the cofactor matrix for the reduced system and use the matrix identity.

$$\begin{aligned} \mathbf{Q_{x_1x_1}} &= \mathbf{N_{11}^{-1}} + \left[\mathbf{N_{11}^{-1} N_{12}} \left(\mathbf{N_{22}} - \mathbf{N_{21} N_{11}^{-1} N_{12}} \right)^{-1} \right. \\ &\qquad \left. \mathbf{N_{21} N_{11}^{-1}} \right] \\ \mathbf{Q_{x_1x_1}} &= \tilde{\mathbf{Q}}_{\mathbf{x_1x_1}} + \bar{\mathbf{Q}}_{\mathbf{x_1x_1}} \end{aligned} \tag{13}$$

The cofactor matrix of the unknowns $\mathbf{Q_{x_1x_1}}$ includes the complete stochastic information according to equation (12) caused of the substitution. The matrix $\bar{\mathbf{Q}}_{\mathbf{x_1x_1}}$ contains the complete information of the substituted clock parameters as an correction. With this concept we can determine the impact of additional unknowns to the estimation of unknown PCV parameters.

Based on (13) correlation matrices for different spherical harmonic expansions can be calculated and compared. We now compare two different expansions $(3,3)$ and $(8,8)$ for a typical calibration scenario of GPS L1 and L2, cf. Figure 5. The correlation matrix for an expansion of $m = n = 3$ is depicted in Figure 5b, for an expansion of $m = n = 8$ in Figure 5c, respectively.

It can be seen that $\mathbf{K_{ff}}$ has a block structure as schematically indicated in Figure 5a. The blocks correspond to the L1 and L2 frequencies respectively. The matrix $\mathbf{K_{f_1f_2}}$ indicates the inter-frequency correlations. The unknown parameters are sorted, first all $\bar{A}_{nm}$ followed by $\bar{B}_{nm}$.

For an expansion $m = n = 3$ correlations of up to 99% appear (cf. Figure 5b). Especially parameters, like e.g., (A_{10}, A_{20}), (A_{11}, A_{21}) and (A_{30}, A_{20}) are highly negative correlated. For the coefficients of $\bar{B}_{nm}$ the same systematic appears, e.g. (B_{11}, B_{21}), (B_{31}, B_{21}). Otherwise some coefficients show high positive correlation, like e.g., (A_{10}, A_{30}), (A_{11}, A_{31}) as well as (B_{11}, B_{31}). These systematic is to be continued by increasing the degree and order of spherical harmonic expansion, as depicted exemplarily for an expansion of $n = m = 8$ (cf. Figure 5c). Low correlations in the range of 1 - 3% appear for mixed $\bar{A}_{nm}$ and $\bar{B}_{nm}$ coefficients.

The matrix $\mathbf{K_{f_1f_2}}$ shows additional inter frequency correlations of up to 10%. They are caused by the differential receiver clock error that links the L1 and L2 observations.

If applying a multi-GNSS approach by expanding the methodology to GLONASS PCV parametrization, the block structure of the correlation matrix is continued, cf. Figure 6. The inter-frequency correlations caused by the consideration of the differential receiver clock error remain unchanged. These correlations are in the range of up to $7-10\%$. It has to be noticed that additionally inter-system correlations appear. They are in the order of a magnitude of $1-2\%$. Thus these correlation have no significant impact on the estimated unknowns.

2.4 Impact of Covariance Information

Up to now we did not consider the covariance information of the observations, i.e. the weight matrix of observation $\mathbf{P}$ equates the identity matrix $\mathbf{E}$. However mathematical correlations due to single differencing as well as elevation depending weights should be considered.

Based on the covariance matrix of the undifferenced phase observations

$$\mathbf{C_{ll}} = \mathbf{diag}(\sigma_t^2), \tag{14}$$

with the empirical standard derivation σ_t for the observation at epoch t_t the complete covariance matrix for time differenced single differences $\mathbf{C_{\Delta SD}}$ can be calculated by the variance covariance propagation law. With an adequate functional matrix for the time differences,

$$\mathbf{F} = \begin{bmatrix} -1 & 1 & 0 & & & & 0 \\ 0 & -1 & 1 & 0 & & & 0 \\ & 0 & -1 & 1 & 0 & & 0 \\ & & \vdots & & \ddots & & \vdots \\ 0 & 0 & 0 & 0 & 0 & -1 & 1 \end{bmatrix} \tag{15}$$

$$\mathbf{C_{\Delta SD}} = F\, C_{ll} F^T$$

This approach results into a irreducible tridiagonal matrix, which has to be inverted for every satellite. Thanks to the special structure of $\mathbf{C_{\Delta SD}}$ the inverse can be calculated directly and analytically without explicit construction of the covariance matrix of the time differenced single differences.

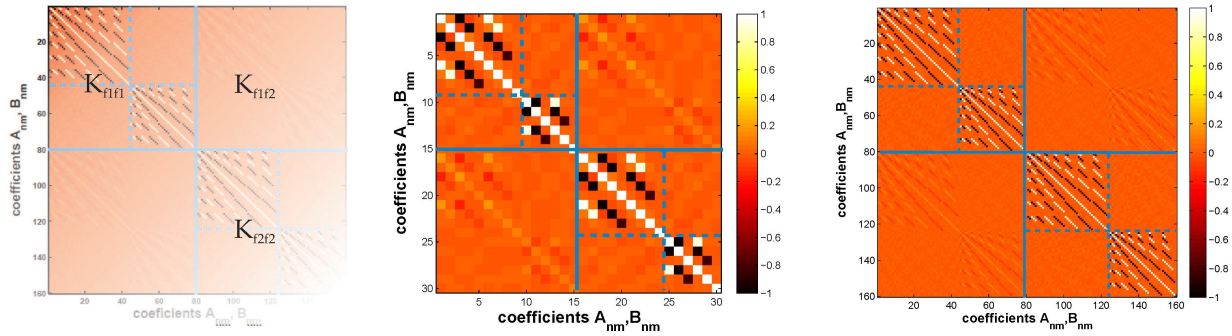

(a) block structure **(b)** 3,3 with clock **(c)** 8,8 with clock

Figure 5. Images of correlation matrices $\mathbf{K_{ff}}$ of different expansions. In the common adjustment of two frequencies one differential receiver clock error per epoch is taken into account. A clear block structure depending on the individual set up of different frequencies can be noticed.

As described in detail by [12] it is only required to know the first and the last column vectors $\vec{u}$ and $\vec{v}$ to calculate the inverse $\mathbf{C}^{-1}_{\Delta\mathbf{SD}}$. For the case of the covariance matrix $\mathbf{C}_{\Delta\mathbf{SD}}$ from equation (15) with equal weighted observations, this yields a tridiagonal band matrix as depicted in Figure 7a.

The inverse of this matrix can be calculated analytically with a simple loop for $\rho \geq \chi$ [12].

$$(\mathbf{C}^{-1}_{\Delta\mathbf{SD}})_{\rho,\chi} = \rho \, \frac{r-\chi+1}{r+1} \tag{16}$$

with $r = c$ (row = columns) being the maximum dimension of $\mathbf{C}_{\Delta\mathbf{SD}}$ and ρ and χ the indices for row and column respectively. An example of the structure of the weight matrix can be found in Figure 7 for 50 epochs.

For an analysis of the impact of the complete covariance information on the correlations the use of $\mathbf{P} = \mathbf{E}$ versus $\mathbf{C}_{\Delta\mathbf{SD}}$

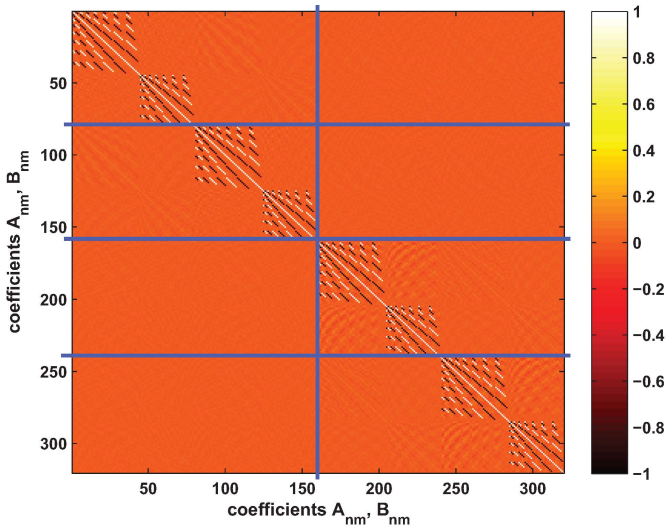

Figure 6. Correlation matrix of combined multi-frequency and multi-GNSS approach. In one common adjustment GLONASS and GPS frequencies L1 and L2 are considered with an additionally clock parameter which is estimated per epoch. The expansion of spherical harmonics is $n = m = 8$.

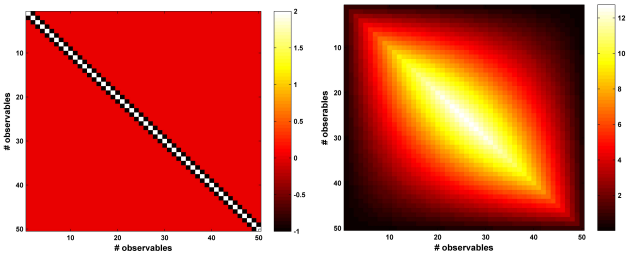

(a) $C_{\Delta SD}$ **(b)** $C^{-1}_{\Delta SD}$

Figure 7. Images of the covariance matrix of time differenced single differences and its inverse are depicted exemplary for 50 epochs. The explicit construction of matrix $\mathbf{C}_{\Delta\mathbf{SD}}$ is not needed.

is compared for $m = n = 8$. For seek of simplicity we consider here in a first step only the so called *geometry* impact for one frequency, i.e. no receiver clock error is estimated. According to the previous analysis, the correlation matrix is computed and the differences to the correlation matrices are depicted in Figure 8.

It can to be seen that the consideration of additional covariance information have an impact of up to 25% on the correlations between the high spherical harmonic coefficients of $\bar{A}_{nm}$ and $\bar{B}_{nm}$ whereas lower order coefficients are not affected. A significant impact is to be recognized on the coefficients $\bar{A}_{n,m=max}$ whereby the impact on the correlations of the $\bar{A}_{n0}$ coefficients vanish. As depicted in Figure 8 block structure appears which is indicated by the combination of even and odd degree of the spherical harmonic coefficients. The sign convention follows a systematics and the degree of correlation and decorrelation depends on degree of the spherical harmonic coefficients, which can be taken form the table 2. For example the combination of even and odd degree yields a positive sign whereby the combination of odd/odd as well as even/even relates to a negative sign for the correlations.

Furthermore it is shown that the higher the order of the coefficients, the higher the expected correlations are, i.e. +11%

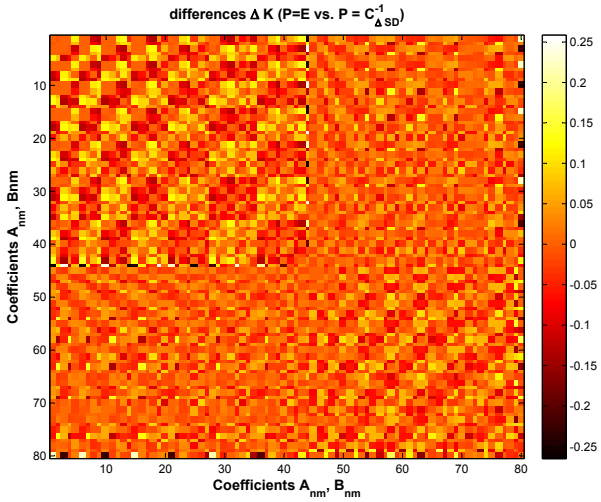

Figure 8. Matrix $\Delta\mathbf{K_{ff}}$ showing the impact of the full covariance information to the estimated spherical harmonic coefficients.

A_{10},A_{22}, +11% (A_{10},A_{43}) and +25% (A_{10},A_{88}).

The values for the impact on coefficients $\bar{B}_{nm}$ are similar to those for $\bar{A}_{nm}$ like e.g. $-2\%\,(B_{63},B_{44})$, $-2\%\,(B_{11},B_{76})$ and $-12\%\,(B_{31},B_{88})$. Please note that the signs for the coefficients $\bar{B}_{nm}$ show not such systematics like for $\bar{A}_{n,m}$.

Table 2. Sign convention for correlation and decorrelation parameter.

degree of coefficients	sign	examples	relativ from	relativ to
even - odd	+	$+11\%A_{10},A_{22})$	+2%	+14%
		$+25\%(A_{10},A_{88})$	0 %	+25%
		$+7\%(A_{55},A_{83})$	-1%	+6%
odd - odd	-	$-10\%(A_{11},A_{33})$	-3%	+13%
		$-10\%(A_{33},A_{52})$	-1%	+11%
		$-12\%(A_{53},A_{70})$	+3%	-8%
even - even	-	$-11\%(A_{22},A_{40})$	-2%	-13%
		$-4\%(A_{22},A_{44})$	-2%	-6%
		$-7\%(A_{22},A_{83})$	+2 %	-6%

Acknowledgement

The authors would like to thank the German Ministry of Economy and Technology (BMWI) and the German Aerospace Center (DLR) as project executing organization for funding this project under the grant 50NA0903.

The current experiments could not have been done without the lending of additional GNSS Equipment. We grateful acknowledge the manufactures Trimble, Topcon and Septentrio who give us the possibility for use their GNSS Equipment during these analysis.

References

[1] Gerhard Wübbena, Martin Schmitz, Falko Menge, Volker Böder, and Guenter Seeber. Automated Absolute Field Calibration of GPS Antennas in Real-Time. In *ION GPS 2000, Salt Lake City, 19-22. September 2000, USA*, 2000.

[2] Bruce R. Schupler, Roger L. Allshouse, and Thomas A. Clark. Signal Characteristics of GPS User Antennas. *Journal of the Institute of Navigation*, 41:277–296, 1994.

[3] Phillip Zeimetz and Heiner Kuhlmann. On the Accuracy of Absolute GNSS Antenna Calibration and the Conception of a New Anechoic Chamber. In *Integrating Generations, FIG Working Week 2008 Stockholm, Sweden 14-19 June 2008*, 2008.

[4] Markus Rothacher, Stefan Schaer, Leos Mervart, and Gerhard Beutler. Determination of Antenna Phase Center Variations using GPS Data. In *Proceedings of IGS Workshop 1995, Potsdam, Germany, May 15-17. 1995*, 1995.

[5] Markus Rothacher. Receiver and Satellite Antenna Phase Center Offsets and Variations. In *IGS Workshop "Towards Real-Time", April 8-11, 2002, Ottawa, Canada*, 2002.

[6] Jim Ray and Ken Senior. Geodetic Techniques for time and frequency comparisons using GPS phase and code measurements. *Metrologia*, 42:215–232, 2005.

[7] Martin Schmitz, Gerhard Wuebbena, and Gerald Boettcher. Absolute GNSS Antenna Calibration with a Robot: Repeatability of Phase Variations, Calibration of GLONASS and Determination of Carrier-to-Noise Pattern. In *IGS Workshop 2006 "Perspectives and Visions for 2010 and beyond", May 8-12, 2006, ESOC, Darmstadt, Germany*, 2006.

[8] Christoph Völksen and Falko Menge. The Impact of different GPS Antenna Calibration Models on the EUREF Permanent Network. In *IAG-EUREF Symposium*, 2002.

[9] H. Dodel and D. Häupler. *Satellitennavigation*. Springer Verlag, 2010.

[10] J.T. Wu, S.C. Wu, G.A. Hajj, W.I. Bertiger, and S.M. Lichten. Effects of antenna orientation on GPS carrier phase. *manuscripta geodaetica, Springer Verlag, New York*, 18:91–98, 1993.

[11] E.W. Hobson. *The Theory of Spherical and Ellipsoidal Harmonics*. Cambridge, University Press, 1931.

[12] Gèrard Meurant. A Review on the Inverse of Symmetric Tridiagonal and Block Tridiagonal Matrices. *SIAM J. Matrix Anal. Applications*, 13:707–728, 1992.